Electronic Supplementary Information

Structure and sum-frequency generation spectra of water on neutral hydroxylated silica surfaces

Konstantin S. Smirnov

Univ. Lille, CNRS, UMR 8516 – LASIRe – Laboratoire Avancé de Spectroscopie pour les Interactions la Réactivité et l'Environnement, F-59000 Lille, France

S1 Computation of system dipole and polarizability

The calculation of spectrum of the resonant part of nonlinear susceptibility $\chi^{(2),R}$ by eq. (6) requires the knowledge of the dipole and polarizability of system. For a slab of water molecules these are obtained by summing up contributions of individual molecules. In the present work, the molecular characteristics were computed in a restricted dipole interaction model (r-DIM).

Dipole interaction model (DIM) considers each molecule as a polarizable point dipole.[1] For a system of N such interacting dipoles, a vector of dipoles $\mathbf{m}$ (length $3N$) can be written as

$$\mathbf{m} = \mathbf{m}^0 + \mathbf{a}(\mathbf{E}^0 + \mathbf{T}\mathbf{m}) \tag{S1}$$

where $\mathbf{m}^0$ is vector non-interacting dipoles, $\mathbf{a}$ stands for matrix of dipole's polarizabilities, the $\mathbf{T}$ matrix is built of dipole-dipole interaction tensors, and $\mathbf{E}^0$ is a vector of external electric field. The solution of (S1) is given by[1,2]

$$\mathbf{m} = \mathbf{m}^0 + \mathbf{a}^{\text{eff}}(\mathbf{E}^0 + \mathbf{T}\mathbf{m}_0), \tag{S2}$$

where

$$\mathbf{a}^{\text{eff}} = \mathbf{a}(\mathbf{1} - \mathbf{T}\mathbf{a})^{-1}. \tag{S3}$$

From the computational viewpoint, the inversion of $3N \times 3N$ matrix in (S3) is clearly the limiting step of model efficiency. To overcome the bottleneck, r-DIM takes the matrix of effective polarizabilities as $\mathbf{a}^{\text{eff}} = \mathbf{a}$ and the computation of molecular dipoles is then performed as

$$\mathbf{m} = \mathbf{m}^0 + \mathbf{a}(\mathbf{E}^0 + \mathbf{T}\mathbf{m}_0), \tag{S4}$$

where the quantities in $\mathbf{m}^0$ and $\mathbf{a}$ are obtained with models described in ref. 3.

Figure S1 displays distributions of mean polarizability and dipole values of molecules in bulk liquid water computed with DIM and r-DIM. The data were obtained for a system of 500 SPCFw molecules in an MD simulation for a temperature of 293 K. One sees in Fig. S1a that the local field correction has a relatively small influence on the polarizabilities. Figure S1b shows that despite an underestimation of dipole values by *ca.* 10 %, the r-DIM model correctly captures the increase of dipoles due to the external field,.

Figure S2 compares $\chi^{(2),R}_{\parallel\parallel\perp}$ spectra for the water/vapor interface obtained with the two models. One sees that taking $\mathbf{a}^{\text{eff}} = \mathbf{a}$ in (S2) has a little impact on both the shape and intensity of the spectra that justifies the simplification.

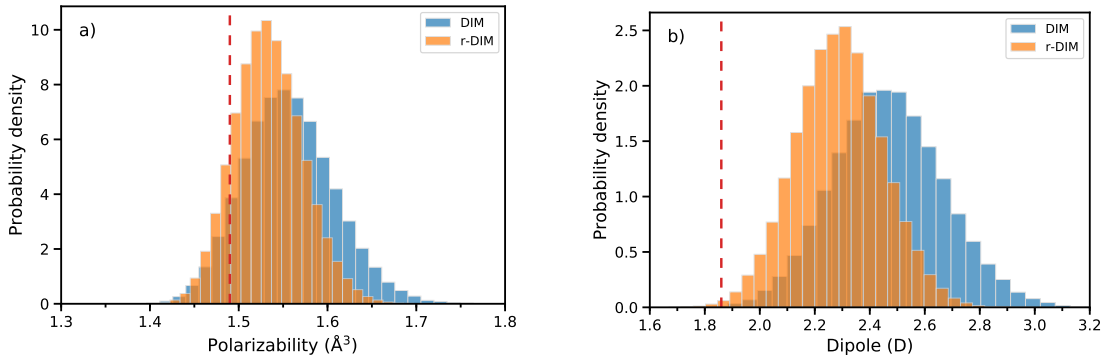

Figure S1: Distributions of mean polarizabilities (a) and dipoles of molecules in bulk liquid water computed for a system of 500 SPCFw molecules in DIM and r-DIM. Vertical red dashed lines indicate the quantity values of an isolated water molecule.

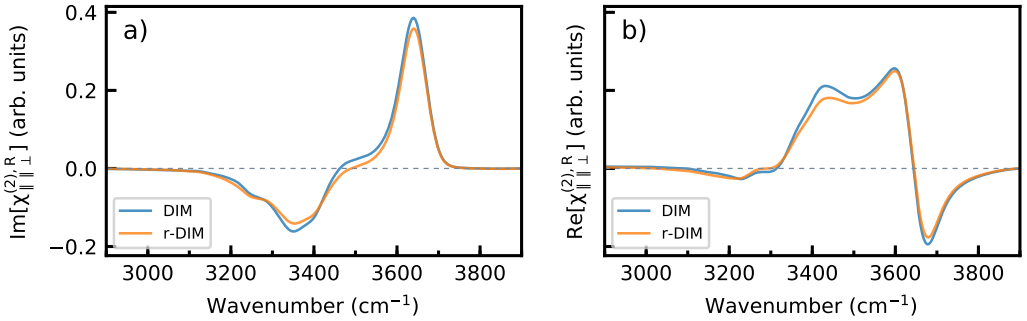

Figure S2: Spectra of imaginary (a) and real (b) parts of nonlinear susceptibility $\chi^{(2)}_{|||\perp}$ computed for water/vapor interface in DIM and r-DIM models.

S2 Comparison of results obtained for the CRB/NW interface in two setups of MD cell

Figure S3 compares z-profiles of the density ρ^* and orientational order parameters S_2 computed in two setups of MD simulation cell for the CRB/NW interface. Figure S4 and Figure S5 present two-dimensional probability maps $Q(r, u, \mathcal{Z})$ (3) and $\tilde{P}(u_1, u_2, \mathcal{Z})$ (4) computed for the system in the two layouts. Finally, Figure S6 displays the $\mathrm{Im}[\chi^{(2),R}_{|||\perp}]$ spectra obtained in the two setups for different interfacial regions.

The comparison of the results in Fig. S3 – Fig. S6 shows an excellent agreement of both the structural characteristics and nonlinear spectra computed in the two setups. Small differences between the results visible in Fig. S3 and Fig. S6 can be ascribed to a limited statistical averaging.

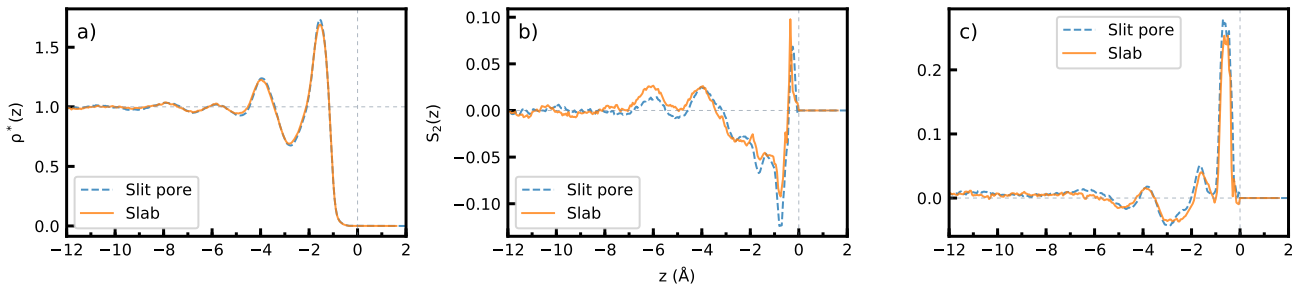

Figure S3: z-profiles of the relative density (a) and of the orientational order parameter S_2 for dipole (b) and HH vector (c) computed in two setups of simulation cell for the CRB/NW interface, see main article for details.

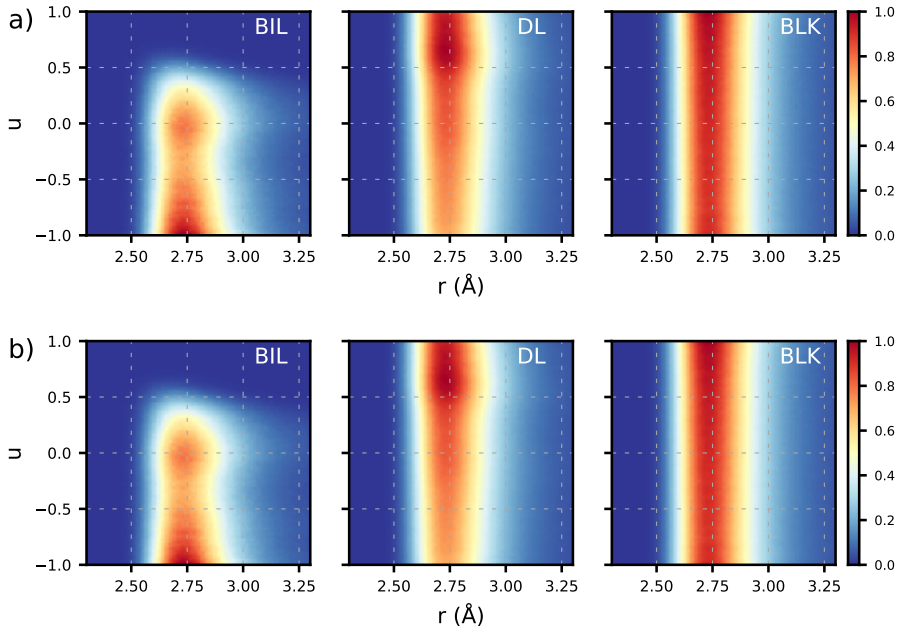

Figure S4: 2D maps of probability distribution $Q(r, u, \mathcal{Z})$ (3) for the CRB/NW interface: a) – slit pore layout, b) – slab layout of simulation cell; $\mathcal{Z}$ regions are indicated with acronyms in the upper right corners.

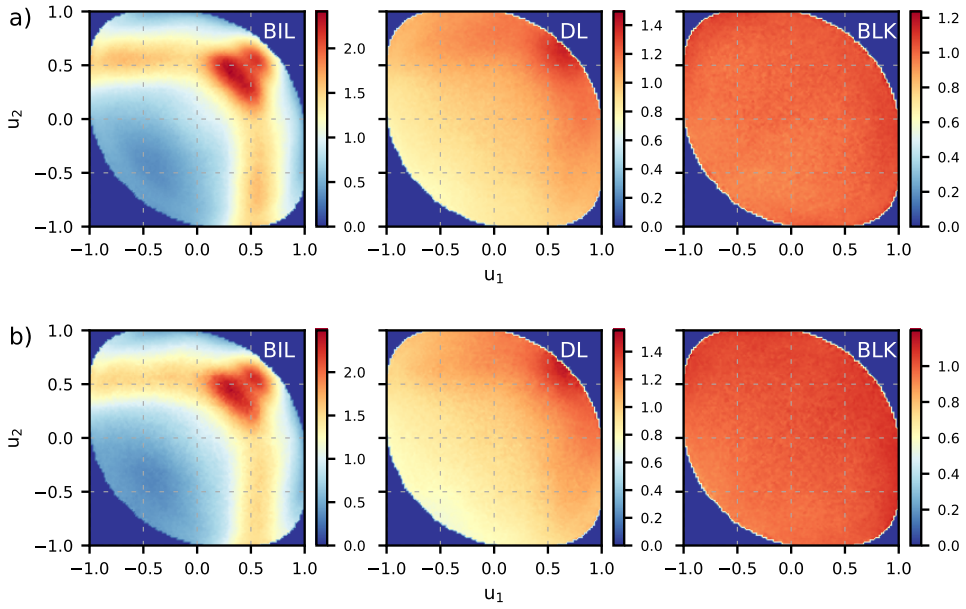

Figure S5: 2D maps of probability distribution $\tilde{P}(u_1, u_2, \mathcal{Z})$ (4) for the CRB/NW interface: a) – slit pore layout, b) – slab layout of simulation cell; $\mathcal{Z}$ regions are indicated with acronyms in the upper right corners.

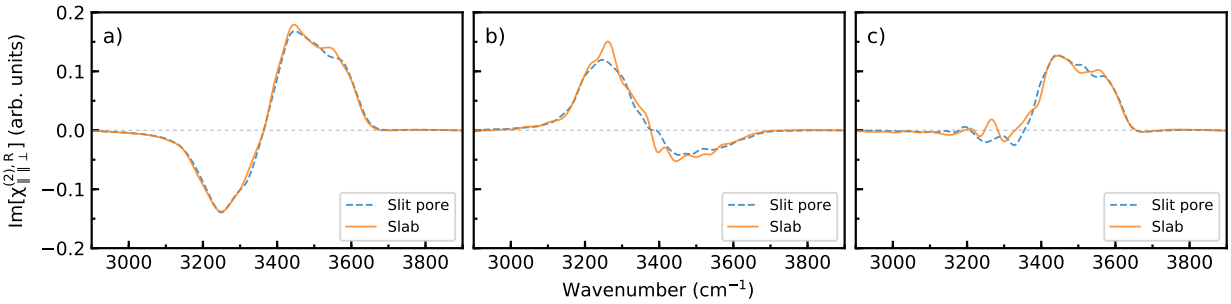

Figure S6: Im$[\chi^{(2),R}_{\parallel\parallel_\perp}]$ spectra for the CRB/NW interface computed in the two layouts of simulation cell. a) – BIL, b) – DL, c) – total interfacial region.

S3 Characteristics of second layer of water on crystalline silica surfaces

Figure S7 and Figure S8 present the two-dimensional maps of joint probability distributions $Q(r, u, \mathcal{Z})$ and $\tilde{P}(u_1, u_2, \mathcal{Z})$, respectively, computed for a second water layer (L2) on the crystalline silica/neat water interface. The L2 layer is easily recognizable in the z-profiles of ρ^* density in Fig. 4 of the main article. Comparison of Figure 10a and Figure 11a (main article) with Figure S7 and Figure S8, respectively, clearly shows that the anisotropic patten in the maps for DL mainly stems from the layer next to BIL of the interfaces.

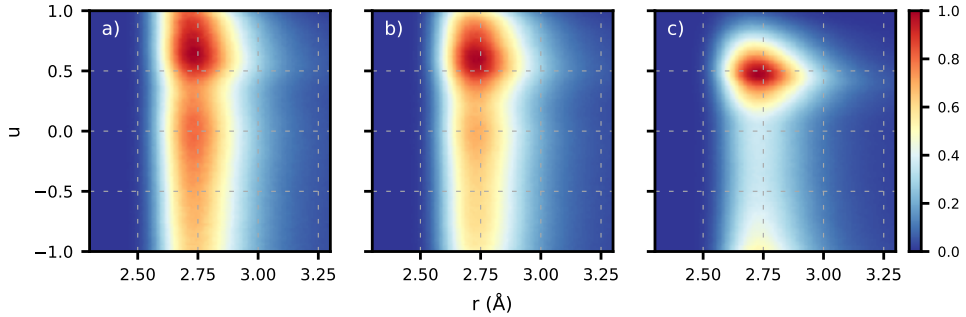

Figure S7: Two-dimensional maps of joint probability distribution $Q(r, u, \mathcal{Z})$ (3) computed for the second water layer on crystalline silica/neat water interfaces: a) – CRB, b) – Q101, c) – Q001.

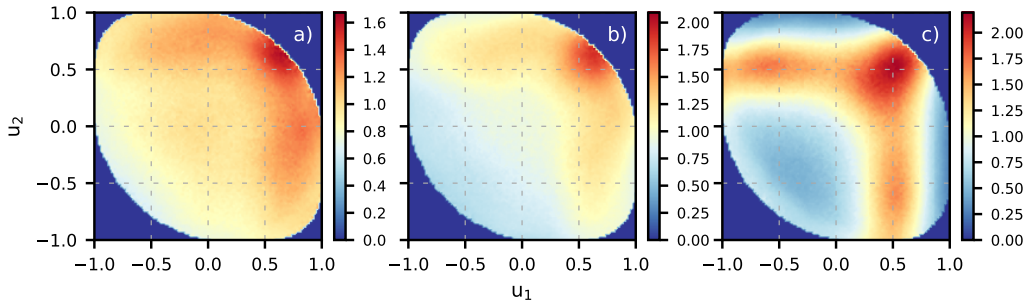

Figure S8: Two-dimensional maps of joint probability distribution $\tilde{P}(u_1, u_2, \mathcal{Z})$ (4) computed for the second water layer of crystalline silica/neat water interfaces: a) – CRB, b) – Q101, c) – Q001.

Figure S9 compares the $\mathrm{Im}[\chi^{(2),R}_{\parallel\parallel\perp}]$ spectra of BIL and DL with the L2 spectrum for the interfaces. From comparison of Fig. S9b and Fig. S9c, one sees that the L2 spectrum, to a large extent, accounts for the spectrum of the diffuse layer. Yet, a part of DL more distant from the surface contributes to the spectrum of the diffuse layer.

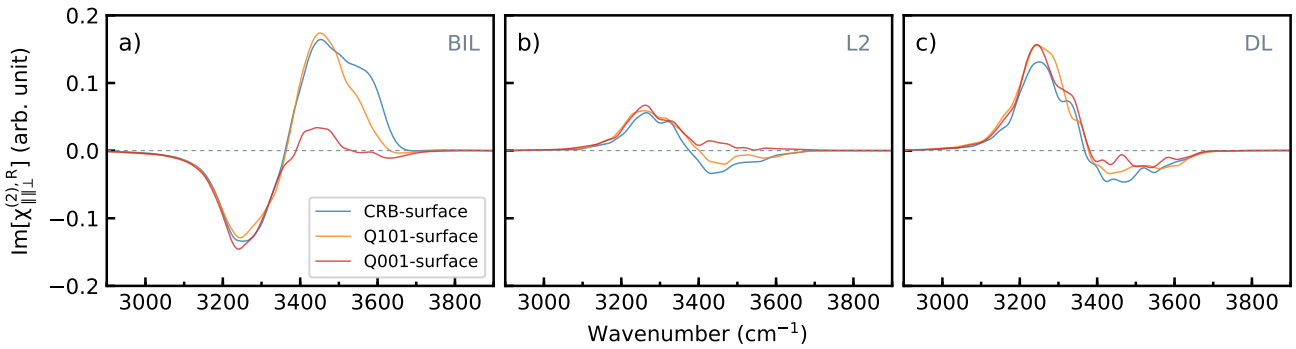

Figure S9: $\mathrm{Im}[\chi^{(2),R}_{\parallel\parallel\perp}]$ computed for the BIL (a), L2 (b) and DL (c) regions of crystalline silica/neat water interfaces.

S4 Density maps of water in BIL of crystalline silica/1 M NaCl solution interfaces

Figure S10 displays maps of water density in the xy-plane in BIL of crystalline silica/1 M NaCl solution interfaces; the maps can be compared with those presented in Fig. 8 of main article. The comparison shows that the presence of ions in solution does not affect the adsorption sites seen in Fig. 8. It should, however, be noted that compared to Fig. 8b, the density map in Fig. S10b reveals adsorption sites in proximity of inner OH groups (see a red circle in Fig. 8b), similar to the second type of adsorption sites found in ref. 4 for water on the Q101 surface. It seems that in the case of the surface, the ions reduce mobility of some water molecules and stabilize their H-bonding to the IN silanols.

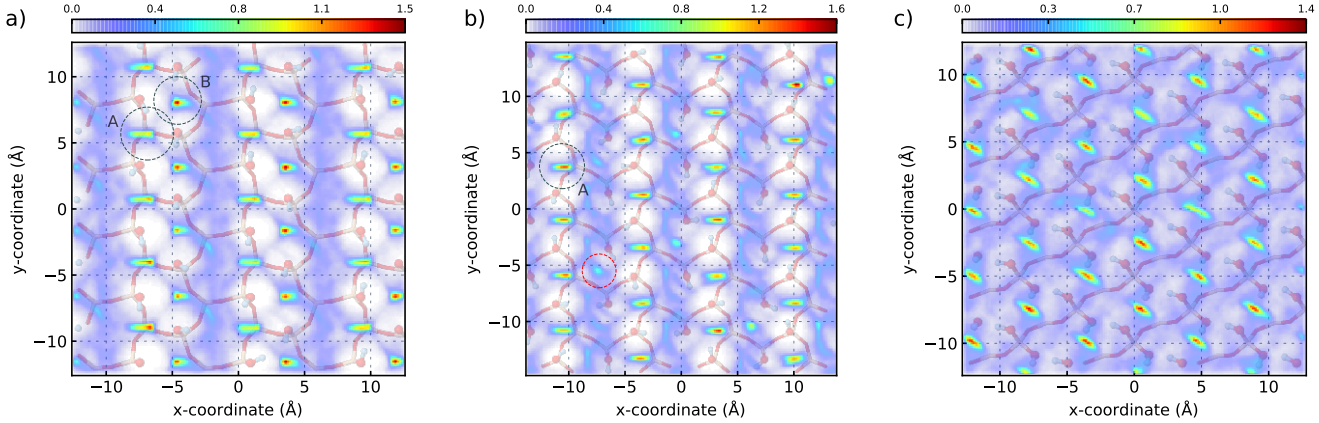

Figure S10: Density maps of water in the xy plane in BIL of crystalline silica/1 M NaCl solution interfaces: a) – CRB/ES, b) – Q101/ES, c) – Q001/ES; quantity used in the maps construction is $\ln(1+\rho^*)$. Dashed circles labelled A and B in the panel (a) indicate two adsorption sites discussed in the text of main article. Dashed circle A in the panel b) shows an adsorption site akin to the site in the pannel a), whereas a red dashed circle marks a second type of adsorption sites, see text.

S5 Mobility characteristics of interfacial water

The mobility of water molecules was characterized by the parallel-to-surface diffusion coefficient (D_{xy}) and the rotational relaxation time of molecular dipole ($\tau_\mu^{(2)}$). The quantities were obtained from the analysis of the mean-squared displacement of molecules in the xy-plane ($MSD_{xy}(t)$) and of the dipole rotational time correlation function $C_2^\mu(t)$, respectively,

$$MSD_{xy}(t) = \langle (x(t) - x(0))^2 + (y(t) - y(0))^2 \rangle \tag{S5}$$

$$C_2^\mu(t) = \langle P_2(\mathbf{u}(t) \cdot \mathbf{u}(0) \rangle, \tag{S6}$$

where $P_2()$ stands for the 2nd-order Legendre polynomial and $\mathbf{u}$ is the unit vector along the molecular dipole $\boldsymbol{\mu}$. The angle brackets in (S5) and (S6) denote averaging over time-origins and over molecules that did not leave the target $\mathcal{Z}$-region for a time longer than 2 ps. Applying the Einstein relationship $MSD_{xy}(t) = 4D_{xy}\,t + C$ yields the diffusion coefficient D_{xy}. The $C_2^\mu(t)$ was fitted by Kohlrausch-Williams-Watts stretched-exponential function $f_{KWW}(t)$

$$f_{KWW}(t) = \exp((-t/T_{KWW})^\gamma) \tag{S7}$$

from which the relaxation time $\tau_\mu^{(2)}$ was obtained as

$$\tau_\mu^{(2)} = \int_0^\infty dt\, f_{KWW}(t) = \frac{T_{KWW}}{\gamma}\Gamma\left(\frac{1}{\gamma}\right), \tag{S8}$$

where $\Gamma()$ stands for the gamma function.

S6 Intrinsic $\chi^{(2)}$ spectrum of diffuse layer

In order to find out whether DL of a solid/water interface has a nonzero $\chi^{(2)}_{\parallel\parallel\perp}$ susceptibility in the absence of surface electric field, the following numerical experiment was conducted. 1152 SPCFw water molecules were enclosed between two surfaces of graphite slab of ten graphene layers. Dimensions of the simulation cell were 29.532 Å, 29.8382 Å and 73.4731 Å along the x-, y- and z-axis, respectively. The interactions between the molecules and the carbon atoms were described with a Lennard-Jones (12–6) potential with parameters taken from ref. 5. In a first series of simulations, hereafter labelled as "Series 1", all interaction parameters had their original values. In the second series referred to as "Series 2", the D_0 parameter (depth of potential) of the C–Ow atoms pair was multiplied by four for H_2O molecules of the first interfacial layer (BIL), while all other parameters were left unchanged. The stronger interaction between the BIL molecules and the surface limited their mobility and the "sticky" H_2O layer mimicked BIL of a silica/water interface.

Simulations of "Series 1" were carried out as described in Section 3.3 of main article. The computational protocol of "Series 2" simulations was slightly different. First, the final configuration of the "Series 1" runs was used to identify BIL water molecules and the C–Ow interaction parameter were changed for these molecules as discussed above. Then, 50 MD simulations of 160 ps length starting from the configuration were performed to produce results for "Series 2". The initial velocities in each of these runs were set independently and the first 120 ps (240000 time-steps) were used as an equlibration stage. The scheme allowed a better sampling the phase space while preserving "sticky" BIL at time $t = 0$ in each run. The simulations were performed for $T = 293$ K.

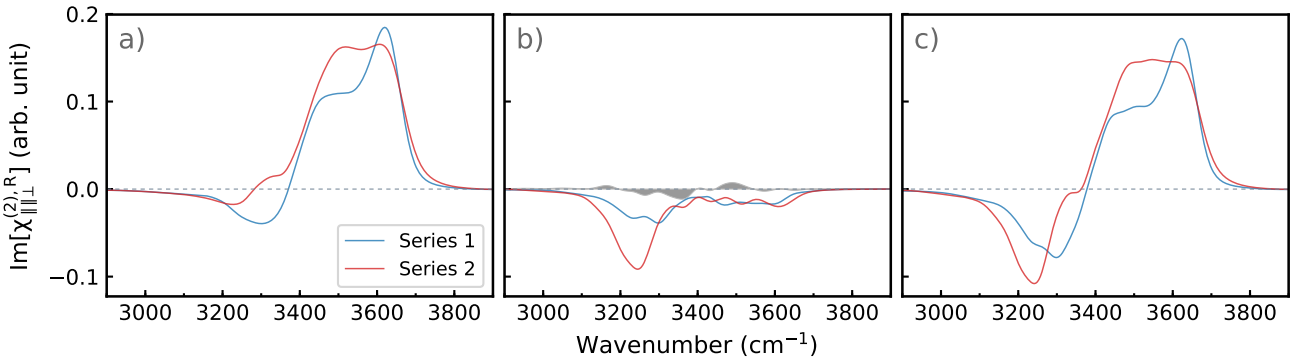

Figure S11: Im[$\chi^{(2),R}_{\parallel\parallel\perp}$] spectra computed for the different interfacial regions of the graphite/water system in the two series of MD simulations as explained in the text, a) – BIL, b) – DL, c) – total interfacial region. Shaded contour in the panel b) shows the spectrum of the bulk region.

Figure S11 presents Im[$\chi^{(2),R}_{\parallel\parallel\perp}$] spectra computed for different regions of the interface in the two series of simulations. The DL spectrum is shown in Fig. S11b and it is characterized by a negative band in a wide wavenumber range from 3100 to 3700 cm^{-1}. One can see that the spectrum has a notable intensity already for the "normal" BIL (Series 1). When BIL molecules become less mobile (Series 2), a low-frequency part of DL spectrum grows in intensity and its minimum shifts to lower wavenumbers. This leads to a downward shift of the negative band in the spectrum of the total interfacial region, Fig. S11c. A gray shaded contour in Fig. S11b shows Im[$\chi^{(2),R}_{\parallel\parallel\perp}$] spectrum calculated for the bulk region. As water structure in this region is isotropic, the intensity of the calculated spectrum can be used as an estimation of intensity error due to finite size effects, insufficient sampling, *etc.* Figure S11b clearly shows that the intensity of DL spectrum in both the series of simulations is largely superior this error estimate.

References

[1] J. Applequist, J. R. Carl, and K.-K. Fung. *Atom dipole interaction model for molecular polarizability. Application to polyatomic molecules and determination of atom polarizabilities*. **J. Am. Chem. Soc.**, 1972, 94, 2952–2960, doi:10.1021/ja00764a010.

[2] A. Morita and J. T. Hynes. *A theoretical analysis of the sum frequency generation spectrum of the water surface. II. Time-dependent approach*. **J. Phys. Chem. B**, 2002, 106, 673–685, doi:10.1021/jp0133438.

[3] K. S. Smirnov. *Structure and sum-frequency generation spectra of water on uncharged Q_4 silica surfaces: a molecular dynamics study*. **Phys. Chem. Chem. Phys.**, 2020, 22, 2033–2045, doi:10.1039/C9CP05765J.

[4] O. Kroutil, Z. Chval, A. A. Skelton, and M. Předota. *Computer simulations of quartz (101)-water interface over a range of pH values*. **J. Phys. Chem. C**, 2015, 119, 9274–9286, doi:10.1021/acs.jpcc.5b00096.

[5] Y. Wu and N. R. Aluru. *Graphitic carbon-water nonbonded interaction parameters*. **J. Phys. Chem. B**, 2013, 117, 8802–8813, doi:10.1021/jp402051t.